





Convection in the active layer speeds up permafrost thaw in coarse-grained soils

M. Magnani ^{1,2,3,*} S. Musacchio ^{3,4} A. Provenzale ^{1,2} and G. Boffetta ^{3,4}

¹*Institute of Geosciences and Earth Resources, National Research Council (CNR-IGG), 10125 Torino, Italy*

²*National Biodiversity Future Center, 90133 Palermo, Italy*

³*INFN, Sezione di Torino, 10125 Torino, Italy*

⁴*Dipartimento di Fisica, Università degli Studi di Torino, 10125 Torino, Italy*



(Received 13 February 2024; revised 9 May 2024; accepted 17 July 2024; published 19 August 2024)

Permafrost thaw is a major concern raised by the ongoing climate change. An understudied phenomenon possibly affecting the pace of permafrost thaw is the onset of convective motions within the active layer caused by the density anomaly of water. Here we explore the effects of groundwater convection on permafrost thawing using a model that accounts for ice-water phase transitions, coupled with the dynamics of the temperature field transported by the Darcy's flow across a porous matrix. Numerical simulations of this model show that ice thawing in the presence of convection is much faster than in the diffusive case and deepens at a constant velocity proportional to the soil permeability. A scaling argument is able to predict correctly the asymptotic velocity. Since in the convective regime the heat transport is mediated by the coherent motion of thermal plumes across the thawed layer, we find that the depth of the thawing interface becomes highly heterogeneous.

DOI: [10.1103/PhysRevFluids.9.L081501](https://doi.org/10.1103/PhysRevFluids.9.L081501)

Introduction. The thawing of permafrost—ground that has been frozen for at least two consecutive years—poses important societal and climatic challenges owing to its control on soil stability, health hazards, and mobilization of compounds trapped in cold soils [1–4]. Permafrost evolution is deeply tied to the thermal and hydrological dynamics at ground surface and within the so-called active layer, that is, the surface layer subject to annual thawing and freezing usually present above permafrost. The dynamics of both the permafrost and the active layer are mostly estimated on the basis of models [5,6], while direct measurements are rather sparse and spotty [2,6].

Climate models mostly project permafrost evolution accounting for the vertical conductive heat transfer across the active layer [7–11]. Nonetheless, a crucial role in determining the speed of permafrost thaw can be played by fluid convection in the active layer soil matrix at large permeability, sustained by the density anomaly of water. During the thawing process, the temperature within the active layer decreases with depth from the surface value to the freezing temperature met at the contact with the permafrost. Across this thermal profile, fluid density varies nonlinearly [Fig. 1(a)]: Below $T \simeq 4^\circ\text{C}$ water has a negative thermal expansion coefficient, i.e., its density increases with temperature, whereas above this value the temperature-density relationship is inverted. Therefore, in the lower part of the active layer where $0^\circ\text{C} < T < 4^\circ\text{C}$, soil water is unstably stratified and convection can occur.

In this work we study the effect of active layer fluid motion on permafrost thaw. We consider an homogeneous-isotropic porous medium saturated with water in the presence of gravity. For the application to permafrost thaw, we assume that the lower part of the domain is frozen (at temperature

*Contact author: marta.magnani@unito.it

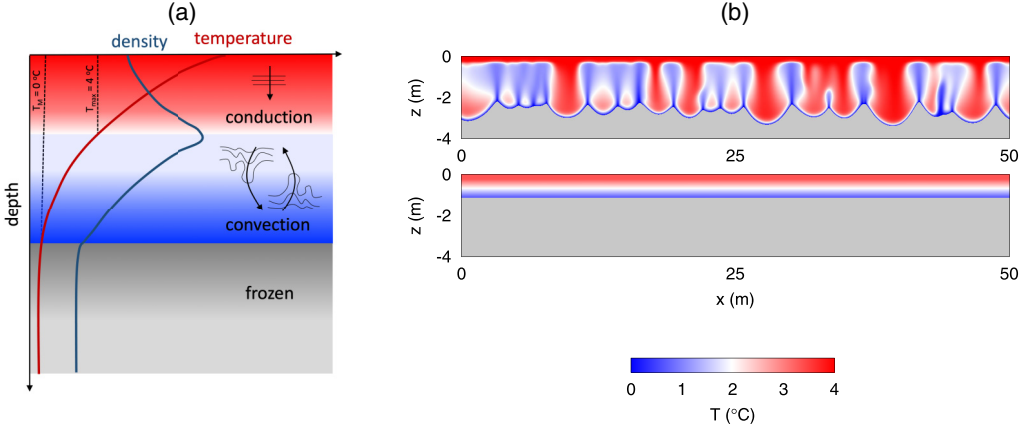


FIG. 1. (a) Schematic dynamics of the active layer considered in this work. In the top layer, where $T > 4^\circ\text{C}$, the fluid stratification is stable, resulting in a diffusive heat transfer. Below this layer the unstable stratification can produce a convective layer characterized by the presence of thermal plumes. The permafrost layer where $T < 0^\circ\text{C}$ is shown in gray. Conceptual representations of temperature and density water profiles are shown with the red and blue lines, respectively. (b) Vertical sections of the temperature fields for runs C (upper panel) and D (lower panel) at time $t = 150$ days, starting from the same initial conditions. Colors indicate the temperature field. The gray area represents the frozen region where $\phi = 1$.

$T_0 < T_M = 0^\circ\text{C}$) while an upper thin porous layer is already melted and in contact to the surface at a temperature $T_1 > T_M$ [see the scheme in Fig. 1(a)]. Three-dimensional direct numerical simulations of this system show that, depending on the permeability of the porous medium, convective motions can develop in the active layer. This accelerates substantially the thawing process with respect to the diffusive behavior and produces a complex water-ice interface which deepens ballistically in time.

Mathematical model and numerical simulations. The physics of thawing in a porous medium is described by a phase field method, a convenient numerical tool for simulating the dynamics of multiphase fluids in the presence of phase transitions [12–14]. The physical state of water is represented by a continuous phase field $\phi(\mathbf{x}, t)$ which takes the value $\phi = 0$ in the liquid phase and $\phi = 1$ in the solid (ice) phase. The equation for the phase field is a Allen-Cahn-type equation [15] coupled with an advection-diffusion equation for the temperature field $T(\mathbf{x}, t)$ and the Darcy’s equation, which describes the velocity field $\mathbf{u}(\mathbf{x}, t)$ in the porous medium,

$$\mathbf{u} = \frac{k}{\mu\phi} (-\nabla p + (1 - \phi)^2 \mathbf{g}\rho) \quad (1)$$

$$\frac{\partial T}{\partial t} + \mathbf{u} \cdot \nabla T = \kappa \nabla^2 T + \Delta T \text{St} \frac{\partial \phi}{\partial t} \quad (2)$$

$$\frac{\partial \phi}{\partial t} = \frac{6\kappa'}{5\text{St}} \left[\nabla^2 \phi - \frac{1}{\delta^2} \phi(1 - \phi) \left(1 - 2\phi + \frac{T - T_M}{\Delta T} \right) \right], \quad (3)$$

where $\mathbf{g} = (0, 0, -g)$ represents gravity, k is the permeability, μ is the fluid viscosity, ϕ the porosity, p is the total pressure, and κ represents an effective thermal diffusivity (linear combination of the solid and the liquid contributions [16]); $\text{St} = L/(c_p \Delta T)$ is the dimensionless Stefan number defined in terms of the latent heat for unit mass L , the specific heat capacity of water c_p , and the temperature jump $\Delta T = T_1 - T_0$, while δ and κ' represent the interface thickness and mobility. Finally, density and temperature of water are related by the empirical nonmonotonic model, valid around the temperature $T_{\max} = 3.98^\circ\text{C}$ of maximal density, $\rho = \rho_0(1 - \alpha^*|T - T_{\max}|^q)$, where α^* is a generalized thermal expansion coefficient, $q = 1.895$, and $\rho_0 = 999.97 \text{ kg/m}^3$ [17]. We remark that the model (1)–(3) assumes local thermal equilibrium by which a single temperature field

describes the solid and the fluid phases in the porous medium [18]. More complex, nonequilibrium, models which take into account heat exchanges within the solid matrix have been proposed [16,19] and could be used for future studies in the present setup.

Because of the density anomaly, the thawed water has an unstable density stratification in the layer where $T_M < T < T_{\max}$. The dimensionless number which controls the dynamics of this fluid layer is the Rayleigh-Darcy number

$$\text{Ra} = \frac{g\Delta\rho kH}{\varphi\mu\kappa}, \quad (4)$$

where H and $\Delta\rho$ are respectively the thickness of and the density difference in the convective layer. For values of Ra below the critical value $\text{Ra}_c = 4\pi^2$, the heat transfer across the active layer is diffusive and the fluid is at rest [20]. In contrast, when $\text{Ra} > \text{Ra}_c$ the unstable density stratification causes a convective motion which displaces the fluid and the temperature field.

We performed direct numerical simulations of Eqs. (1)–(3) by a fully parallel (MPI) pseudospectral code up to resolution $2048 \times 2048 \times 512$. Boundary conditions on the top and bottom layers are imposed by penalization terms, while we use periodic condition in the horizontal directions. In all the simulations, the fluid is initially at rest and the vertical temperature profile within the active layer of depth H_0 is a linear ramp, connecting the temperature $T_0 = -1^\circ\text{C}$ in the permafrost bulk to $T_1 = T_{\max}$ at the ground surface. In order to destabilize the flow, a small random perturbation is added to the initial fluid temperature profile. Units for space and time are meters and days, respectively, and for the physical parameters we set $\kappa = 0.012 \text{ m}^2/\text{day}$, $\mu = 86.0 \text{ kg}/(\text{m day})$, and $L = 3.3 \times 10^5 \text{ J/kg}$ (for simplicity we use the same values for liquid and ice phase). Three different runs have been performed, all with porosity $\varphi = 0.5$, with permeabilities $k = 4.4 \times 10^{-9} \text{ m}^2$ (A), $k = 5.9 \times 10^{-9} \text{ m}^2$ (B), and $k = 8.8 \times 10^{-9} \text{ m}^2$ (C), typical of water in gravel. As a benchmark, we also consider an additional run with much smaller permeability $k = 6 \times 10^{-11} \text{ m}^2$ (D), which remains in the diffusive regime. The numerical method has been tested in the case of a purely diffusive process, i.e., with $\mathbf{u} = 0$ in (2), corresponding to the standard Stefan problem, for which analytical predictions are available.

Results. Assuming an initial small thickness H_0 , such that $\text{Ra} < \text{Ra}_c$, the early stage of the thawing process is characterized by diffusive heat flux from the surface. Consequently, the width of the liquid layer is expected to increase as $H(t) \propto t^{1/2}$ [21]. This growth is accompanied by the increase of Rayleigh-Darcy number (4), which eventually becomes larger than Ra_c , causing the onset of convection. It is well known that, in general, convection is much more efficient to transfer heat than diffusion, and porous convection is not an exception [22,23]. Therefore, in the convective regime $H(t)$ is expected to grow much faster than in the diffusive case. This results in a further increase of Ra and of the convective motion, which accelerates the thawing process.

A first insight into the difference between the conductive and convective dynamics can be obtained from the active layer temperature field. Figure 1(b) shows two vertical sections on the (x, z) plane of the water temperature field (colors) taken at $t = 150$ days for the conductive case (run D, lower panel) and one convective case (run C, upper panel). The frozen part is represented in gray.

When the permeability is small (run D) the heat transfer in the active layer is purely diffusive, resulting in a uniform temperature gradient in the liquid layer and a flat fluid-ice interface. Conversely, the convective cases [such as run C in Fig. 1(b)] are characterized by the presence of thermal plumes that are responsible for the efficient exchange of heat across the active layer and speed up the thawing process. Thermal plumes are generated close to the layer at temperature T_{\max} and they move downwards causing an inhomogeneous heating and thawing of the ice. As a consequence, the fluid-ice interface is not flat, and ice and water coexist at a given depth z , in clear contrast with the diffusive case [compare the top and bottom simulation in Fig. 1(b)].

Thermal plumes that have reached different depths in the thawing process create complex patterns at the *thawing surface* $h(x, y, t)$, defined in this study as the depth where the local phase field $\phi(\mathbf{x}, t) = 1/2$. One example of this surface is shown in Fig. 2(a) for run C at time $t = 150$ days. The average depth reached by convection is in this case $H(t) \simeq 1.6 \text{ m}$, but we observe local

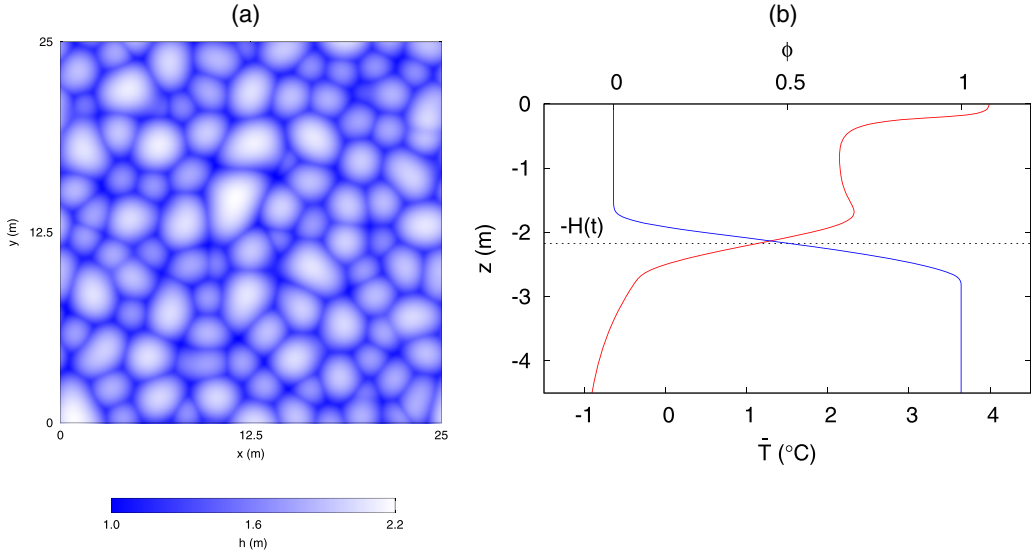


FIG. 2. (a) Thawing surface depth $h(x, y)$, defined from the phase field as the points where $\phi(x, y, h) = 1/2$, for run C at time $t = 150$ days. The average position of the surface is $H = 1.6$ m. (b) Vertical temperature profile $\bar{T}(z)$ (red line) and phase field profile $\bar{\phi}(z)$ (blue line) at time $t = 150$ days. The black dotted line represents the average position of the interface defined as $\bar{\phi}(-H) = 1/2$. Results from run C.

fluctuations ranging from 1 m up to 2.2 m below downwelling plumes. Remarkably, similar patterns have been recently reported as the results of dissolution processes observed both in geological sites and in laboratory experiments in bulk flows [24].

In order to compare quantitatively the conductive and convective processes, we compute the vertical profiles of temperature field $\bar{T}(z)$ and of phase field $\bar{\phi}(z)$, where the overbar represents the average over horizontal planes. Figure 2(b) shows one example of these profiles for run C. In the temperature profile we recognize the presence of a boundary layer close to the upper surface at temperature T_1 , followed by a nonmonotonic temperature pattern, due to the presence of thermal plumes which produce a local temperature maximum. Below this maximum, the temperature decreases sharply, while the phase field profile $\bar{\phi}(z)$ increases. The region in which $0 < \bar{\phi} < 1$ corresponds to the thawing surface with the coexistence, at a given depth, of zones which are liquid ($\phi = 0$) with others still frozen ($\phi = 1$). The depth at which $\bar{\phi}(z) = 1/2$ is used to define the average vertical position $H(t)$ of the water-ice interface (dotted line in Fig. 2(b)).

The displacement of the interface $H(t)$ as a function of time is shown in Fig. 3(a). The convective case with lowest permeability (run A, green line) is initially below the critical Rayleigh-Darcy number and therefore in a first phase it follows the diffusive Stefan solution (gray line). At about $t = 15$ days convection sets in and the displacement of the interface accelerates with respect to the diffusive case. For larger values of the permeability [run B (red line) and run C (blue line)] the convective motion develops since the beginning. The effect of convection on the thawing process is evident: After 60 days (vertical dashed line) the interface has displaced, in the case of the highest permeability, of about 0.7 m from the starting position, which is more than three times what is predicted in the absence of convection (gray line).

At long times, the convection-driven motion of the interface attains a linear law $H \propto t$, instead of the diffusive growth predicted by the Stefan model. This can be understood from the mathematical model governing the process. From the Darcy equation (1) one can define a characteristic velocity $U_0 = \Delta\rho kg/(\mu\varphi)$, which represents the typical speed of thermal plumes. By rescaling the different trajectories of $H(t)$ in Fig. 3(a) with U_0 one obtains the collapse on the linear behavior $H(t) = \alpha U_0 t$

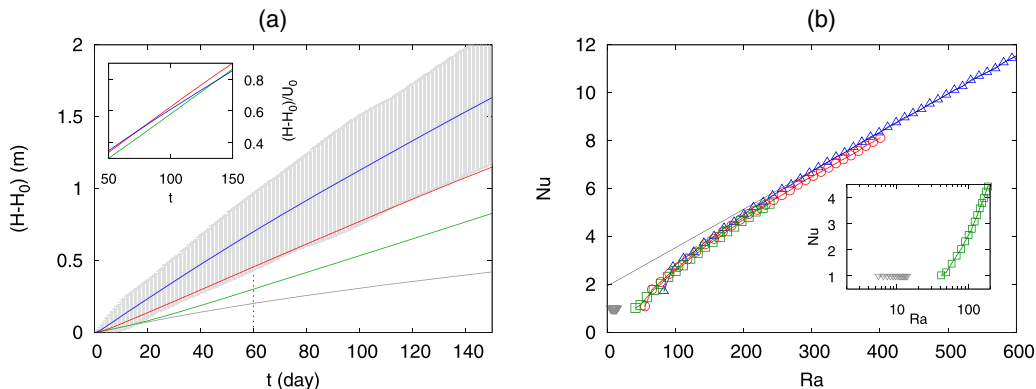


FIG. 3. (a) Average displacement of the water-ice interface as a function of time for the three runs in the convective regime A (green line), B (red line), and C (blue line) and for run D in the diffusive regime (gray line). $H_0 = 0.33$ m is the initial position of the interface at $t = 0$. The gray area represents the width of the thawing layer ($0 < \bar{\phi}(z) < 1$) for run C. The vertical dashed line is a guide for the $t = 60$ days. Inset: Displacement rescaled with the characteristic velocity U_0 in the last part of the evolution. (b) Nusselt number Nu as a function of the Rayleigh-Darcy number Ra for run A (green squares), B (red circles), C (blue triangles), and D (gray inverted triangles). The black line represent the linear fit $Nu = 0.016 Ra + \text{const}$. Inset: The same data in semilogarithmic scales for the lower range of Ra .

with $\alpha \simeq 0.0055$, as shown in the inset of Fig. 3(a). Hence, by changing the permeability value (or the other parameters in U_0), one obtains different velocities of the thawing interface in the convective regime. We remark that the dimensionless coefficient α is here much smaller than the one observed in Rayleigh-Taylor convection in porous media [23] since a significant fraction of the energy is used to thaw the ice phase.

Together with H , we find that also the extension of the layer where $0 < \bar{\phi}(z) < 1$ grows with time, as shown by the gray area in Fig. 3(a) for run C. This region corresponds to the coexistence of zones that are already liquid ($\phi = 0$) with others still frozen ($\phi = 1$) at a given depth, i.e., the vertical extension of the thawing surface shown in Fig. 2(a).

The enhancement of the heat transport due to the convection with respect to the thermal diffusion is quantified by the Nusselt number Nu , defined as the ratio of the total (convective plus diffusive) heat flux to the diffusive one:

$$Nu = \frac{\langle u_z T \rangle H}{\kappa(T_{\max} - T_M)} + 1, \quad (5)$$

where $\langle \dots \rangle$ indicates the average over the convective region of depth H and u_z is the vertical velocity. Figure 3(b) shows the evolution of the Nusselt number (5) as a function of the Rayleigh-Darcy number (4) for the four runs. We recall that since the thickness of the active layer H grows with time, so does the Rayleigh-Darcy number and therefore each simulation spans a range of Ra . Given the small density differences of water between T_M and T_{\max} , the Rayleigh-Darcy number remains moderate for all the permeability values investigated here. As shown in the inset of Fig. 3(b), the Nusselt number in the run D at the lowest permeability is always $Nu = 1$, because it remains in the diffusive regime ($Ra < Ra_c$). For the other three simulations we see that, for sufficiently large values of the Rayleigh-Darcy number, Nu increases with Ra following a linear law. This can be understood by a scaling argument based on the definitions of the two dimensionless numbers. Indeed, from (4) we see that, at fixed values of the fluid parameters, Ra is proportional to the thickness H of the fluid layer. From Eq. (5), assuming that the correlation between the vertical velocity and the temperature field can be simply expressed as $\langle u_z T \rangle = \beta U_0 \Delta T$ (where β is a dimensionless constant) we have the prediction of a linear scaling $Nu = \beta Ra$, as indeed observed in Fig. 3(b), with $\beta \simeq 0.016$. We

remark that, in spite of the different thawing speed for the different permeability values, Fig. 3(b) indicates a universal $Ra - Nu$ relation, almost independent of the permeability k . This suggests that the correlation between the vertical velocity and the temperature, which enters in Eq. (5), is not affected by the permeability of the porous medium.

Conclusion. To conclude, we have studied how convection accelerates the pace of permafrost thawing compared to the conduction process in gravel-dominated soils. With the onset of convection, the ice-water interface deepens linearly in time, in clear contrast with the diffusive law expected from the conductive case. Another consequence of convection is the formation of a complex thawing interface, characterized by spatial patterns, that can be used as a diagnostic for the presence of convection in the active layer. Remarkably, similar patterns have been observed in dissolution processes in bulk flows [24]. Further investigations are needed to clarify whether the observed thawing surface can be explained within the same theoretical framework.

Convective flows have been already mentioned in Arctic field studies [25–27], thus confirming the possibility of this process in natural conditions. According to the present study, the onset of convection is mostly controlled by the soil permeability. Indeed in saturated soils, large permeability values are needed to reach the condition for the fluid density stratification to become unstable and undergo convective motions. Using typical water parameters, such a condition is met for instance in rocky and sandy-gravel soils [28–30]. Fire events in arctic and subarctic ecosystems have also been suggested to increase the connectivity of soil pores, i.e., soil permeability, thus allowing for advective fluid flows that enhance postfire permafrost degradation [30,31]. Instead, if the active layer is characterized by a soil matrix with low permeability the onset of convection is usually prevented.

Despite using a simplified representation of the active layer system, where for instance soil characteristics are kept constant in time and across soil depths, we showed the importance of considering convective processes in cold soils as their effects can already manifest on short timescales of the order of 1 month. Hence, the effects of convection can already be felt within one summer period, when the ground surface temperature can be much higher than 4 °C. These results suggest that climate models accounting for only heat conduction may underestimate the permafrost thawing depth in most permeable soils, where soil water convection in the active layer can occur. In these cases, the framework proposed here may serve to obtain useful parametrizations to be implemented in climate models.

Acknowledgments. We acknowledge HPC CINECA for computing resources (INFN-CINECA Grant No. INFN23-FieldTurb). M.M. and A.P. acknowledge the Italian National Biodiversity Future Center (NBFC) National Recovery and Resilience Plan (NRRP; mission 4, component 2, investment 1.4 of the Ministry of University and Research, funded by the European Union - NextGenerationEU; project code CN00000033).

-
- [1] J. Hjort, D. Streletskiy, G. Doré, Q. Wu, K. Bjella, and M. Luoto, Impacts of permafrost degradation on infrastructure, *Nat. Rev. Earth Environ.* **3**, 24 (2022).
 - [2] O. Karjalainen, J. Aalto, M. Luoto, S. Westermann, V. E. Romanovsky, F. E. Nelson, B. Eitzelmüller, and J. Hjort, Circumpolar permafrost maps and geohazard indices for near-future infrastructure risk assessments, *Sci. Data* **6**, 190037 (2019).
 - [3] J. Hjort, O. Karjalainen, J. Aalto, S. Westermann, V. E. Romanovsky, F. E. Nelson, B. Eitzelmüller, and M. Luoto, Degrading permafrost puts Arctic infrastructure at risk by mid-century, *Nat. Commun.* **9**, 5147 (2018).
 - [4] N. Colombo, F. Salerno, S. Gruber, M. Freppaz, M. Williams, S. Fratianni, and M. Giardino, Impacts of permafrost degradation on inorganic chemistry of surface fresh water, *Glob. Planet. Change* **162**, 69 (2018).

- [5] S. E. Chadburn, E. J. Burke, P. M. Cox, P. Friedlingstein, G. Hugelius, and S. Westermann, An observation-based constraint on permafrost loss as a function of global warming, *Nat. Clim. Chang.* **7**, 340 (2017).
- [6] J. Obu, S. Westermann, A. Bartsch, N. Berdnikov, H. H. Christiansen, A. Dashtseren, R. Delaloye, B. Elberling, B. Etzelmüller, A. Kholodov, Northern Hemisphere permafrost map based on TTOP modelling for 2000–2016 at 1 km² scale, *Earth-Science Rev.* **193**, 299 (2019).
- [7] R. Dankers, E. J. Burke, and J. Price, Simulation of permafrost and seasonal thaw depth in the JULES land surface scheme, *Cryosphere* **5**, 773 (2011).
- [8] R. Wania, I. Ross, and I. C. Prentice, Integrating peatlands and permafrost into a dynamic global vegetation model: 1. Evaluation and sensitivity of physical land surface processes, *Global Biogeochem. Cycles* **23**, 3 (2009).
- [9] M. Guimberteau, D. Zhu, F. Maignan, Y. Huang, C. Yue, S. Dantec-Nédélec, C. Ottlé, A. Jornet-Puig, A. Bastos, P. Laurent, ORCHIDEE-MICT (v8. 4.1), a land surface model for the high latitudes: Model description and validation, *Geosci. Model Dev.* **11**, 121 (2018).
- [10] D. M. Lawrence, A. G. Slater, V. E. Romanovsky, and D. J. Nicolsky, Sensitivity of a model projection of near-surface permafrost degradation to soil column depth and representation of soil organic matter, *J. Geophys. Res.: Earth Surf.* **113**, F2 (2008).
- [11] C. G. Andresen, D. M. Lawrence, C. J. Wilson, A. D. McGuire, C. Koven, K. Schaefer, E. Jafarov, S. Peng, X. Chen, I. Gouttevin, Soil moisture and hydrology projections of the permafrost region—A model intercomparison, *Cryosphere* **14**, 445 (2020).
- [12] C. Beckermann, H.-J. Diepers, I. Steinbach, A. Karma, and X. Tong, Modeling melt convection in phase-field simulations of solidification, *J. Comput. Phys.* **154**, 468 (1999).
- [13] B. Favier, J. Purseed, and L. Duchemin, Rayleigh–Bénard convection with a melting boundary, *J. Fluid Mech.* **858**, 437 (2019).
- [14] R. Yang, K. L. Chong, H.-R. Liu, R. Verzicco, and D. Lohse, Abrupt transition from slow to fast melting of ice, *Phys. Rev. Fluids* **7**, 083503 (2022).
- [15] E. W. Hester, L.-A. Couston, B. Favier, K. J. Burns, and G. M. Vasil, Improved phase-field models of melting and dissolution in multi-component flows, *Proc. R. Soc. A* **476**, 20200508 (2020).
- [16] A. Rees and I. Pop, Vertical free convective boundary-layer flow in a porous medium using a thermal nonequilibrium model, *J. Porous Media* **3**, 31 (2000).
- [17] Z. Wang, E. Calzavarini, C. Sun, and F. Toschi, How the growth of ice depends on the fluid dynamics underneath, *Proc. Natl. Acad. Sci. USA* **118**, e2012870118 (2021).
- [18] E. R. Lapwood, Convection of a fluid in a porous medium, *Math. Proc. Camb. Phil. Soc.* **44**, 508 (1948).
- [19] N. Banu and D. A. S. Rees, Onset of Darcy–Benard convection using a thermal non-equilibrium model, *Int. J. Heat Mass Transf.* **45**, 2221 (2002).
- [20] D. A. Nield and A. Bejan, *Convection in Porous Media* (Springer, Berlin, 2006), Vol. 3.
- [21] L. I. Rubenstein, *The Stefan Problem* (American Mathematical Society, New York, 1971), Vol. 27.
- [22] D. R. Hewitt, Vigorous convection in porous media, *Proc. R. Soc. A* **476**, 20200111 (2020).
- [23] G. Boffetta, M. Borgnino, and S. Musacchio, Scaling of Rayleigh–Taylor mixing in porous media, *Phys. Rev. Fluids* **5**, 062501(R) (2020).
- [24] M. Chaigne, S. Carpy, M. Massé, J. Derr, S. Courrech du Pont, and M. Berhanu, Emergence of tip singularities in dissolution patterns, *Proc. Natl. Acad. Sci. USA* **120**, e2309379120 (2023).
- [25] J. Boike, K. Roth, and P. P. Overduin, Thermal and hydrologic dynamics of the active layer at a continuous permafrost site (Taymyr Peninsula, Siberia), *Water Resour. Res.* **34**, 355 (1998).
- [26] J. Weismüller, U. Wollschläger, J. Boike, X. Pan, Q. Yu, and K. Roth, Modeling the thermal dynamics of the active layer at two contrasting permafrost sites on Svalbard and on the Tibetan Plateau, *Cryosphere* **5**, 741 (2011).
- [27] J. Hollesen, B. Elberling, and P.-E. Jansson, Future active layer dynamics and carbon dioxide production from thawing permafrost layers in Northeast Greenland, *Glob. Change Biol.* **17**, 911 (2011).
- [28] T. Gleeson, L. Smith, N. Moosdorf, J. Hartmann, H. H. Dürr, A. H. Manning, L. P. H. van Beek, and A. M. Jellinek, Mapping permeability over the surface of the Earth, *Geophys. Res. Lett.* **38**, L02401 (2011).

- [29] R. P. Chapuis, Predicting the saturated hydraulic conductivity of soils: A review, [Bull. Eng. Geol. Environ.](#) **71**, 401 (2012).
- [30] B. A. Ebel, J. C. Koch, and M. A. Walvoord, Soil physical, hydraulic, and thermal properties in interior Alaska, USA: Implications for hydrologic response to thawing permafrost conditions, [Water Resour. Res.](#) **55**, 4427 (2019).
- [31] S. C. Zipper, P. Lamontagne-Hallé, J. M. McKenzie, and A. V. Rocha, Groundwater controls on postfire permafrost thaw: Water and energy balance effects, [J. Geophys. Res.: Earth Surf.](#) **123**, 2677 (2018).